Probabilistic Models for the Tensile Strength of Corroding Strands in Posttensioned Segmental Concrete Bridges

Radhakrishna G. Pillai[1]; Paolo Gardoni, M.ASCE[2]; David Trejo, P.E., M.ASCE[3]; Mary Beth D. Hueste, P.E., M.ASCE[4]; and Kenneth F. Reinschmidt, P.E., M.ASCE[5]

Abstract: The presence of air voids, moisture, and chlorides inside tendon systems on segmental posttensioned (PT) bridges has been cited as a reason for the early age corrosion and failure of strands in these bridges. This paper develops probabilistic models to predict the time-variant tension capacity of PT strands exposed to wet-dry conditions. A total of 384 unstressed and 162 stressed strand test specimens were exposed to various void, moisture, and chloride conditions for 0, 12, 16, and 21 months; the residual tension capacities of the strands were then determined. Using these experimental data, a Bayesian approach is used to develop probabilistic capacity models for unstressed and stressed strands. The tension capacities of stressed strands under potential void, wet-dry, and chloride conditions in the field are predicted using the developed models. Probabilistic time-variant models are formulated in such a way that they can be updated by other researchers using additional information from the testing of unstressed strands only, avoiding expensive and cumbersome testing of stressed strands. The *mean absolute percentage errors* of these models are less than 3.2%, indicating good overall model accuracy.

DOI: 10.1061/(ASCE)MT.1943-5533.0000096

CE Database subject headings: Probability; Tensile strength; Corrosion; Durability; Posttensioning; Prestressing; Voids; Ducts; Bridges; Concrete.

Author keywords: Probability; Tensile strength; Capacity; Corrosion; Durability; Posttensioning; Prestressing strands; Tendons; Stress; Voids; Ducts; Segmental bridges.

Introduction

In the Europe and United States, the construction of posttensioned (PT), segmental, concrete bridges began in the 1950s and 1960s, respectively. Fig. 1 shows a typical cross section of a PT box girder with grouted tendons. NCHRP (1998), ASBI (2000), and FDOT (2001a,b) reported the presence of air voids (voids herein) and corroded strands in the grouted tendons. Schupack (2004) reported that bleed-water evaporation and poor grouting and construction practices are possible reasons for the unwanted void formation inside the ducts of the tendons. The presence of moisture and chlorides inside the voids caused the early age corrosion-induced failures of the PT strands in the Mid-bay, Sunshine Skyway, and Niles Channel bridges in Florida at 8, 13, and 16 years, respectively, after construction (NCHRP 1998; ASBI 2000; FDOT 2001a,b). In addition, Woodward et al. (2001) observed the presence of water and chloride-contaminated grout in approximately 13% of the tendons in 281 PT bridges in the United Kingdom; voids were also present in most of these tendons. The presence of voids, water, and chlorides can cause strand corrosion; resulting in a reduction in the tensile strength or tension capacity of strands C_T. Grouted tendons containing several strands are the major load-carrying elements in PT bridges. Poston et al. (2003) reported that a 25% reduction in the C_T of tendons can result in 50% or more reduction in the live load-carrying capacity of bridges. In short, strand corrosion can lead to a reduction in the structural capacity and reliability of PT bridges.

PTI (1998) defined the *minimum ultimate tensile strength* (MUTS) of a strand as the force equal to the nominal cross-sectional area of a strand multiplied by its nominal ultimate tensile stress (f_{pu}). In general, the MUTS of strands is used for structural design and analysis purposes assuming that the strands are in "as-received" conditions with a negligible amount of corrosion. Typically, a 1,860-N/mm^2 (270-ksi) grade, 15.2-mm-(0.6-in.-) diameter, seven-wire strand with MUTS of 261 kN (58.6 kips) and meeting the ASTM (2006), the *Standard Specification for Steel Strand, Uncoated Seven-Wire for Prestressed Concrete*, specifications is used in PT bridges. However, the strands can corrode and lose strength when exposed to corrosive field conditions for a period of time. Therefore, probabilistic models to predict C_T as a function of exposure conditions and exposure time are necessary to properly assess the time-variant structural capacity and reliability of PT bridges. The exposure conditions include material (i.e., grout), void, stress, and environmental conditions. The following paragraphs provide a review of

[1]Graduate Student, Zachry Dept. of Civil Engineering, Texas A&M Univ., 3136 TAMU, College Station, TX 77843-3136 (corresponding author).

[2]Associate Professor, Zachry Dept. of Civil Engineering, Texas A&M Univ., 3136 TAMU, College Station, TX 77843-3136.

[3]Zachry Career Development Professor I, Zachry Dept. of Civil Engineering, Texas A&M Univ., 3136 TAMU, College Station, TX 77843-3136.

[4]E.B. Snead II Associate Professor, Zachry Dept. of Civil Engineering, Texas A&M Univ., 3136 TAMU, College Station, TX 77843-3136.

[5]J. L. Frank/Marathon Ashland Petroleum LLC Chair in Engineering, Project Management Professor, Zachry Dept. of Civil Engineering, Texas A&M Univ., 3136 TAMU, College Station, TX 77843-3136.

Note. This manuscript was submitted on July 25, 2009; approved on March 4, 2010; published online on March 6, 2010. Discussion period open until March 1, 2011; separate discussions must be submitted for individual papers. This paper is part of the ***Journal of Materials in Civil Engineering***, Vol. 22, No. 10, October 1, 2010. ©ASCE, ISSN 0899-1561/2010/10-967–977/$25.00.

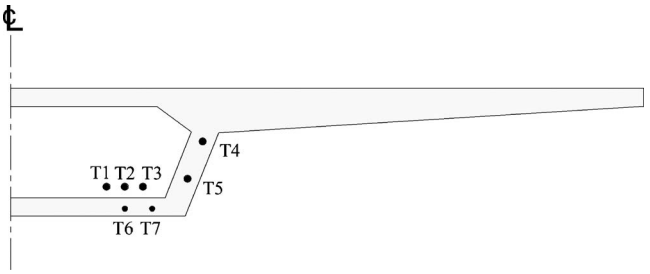

Fig. 1. Typical cross section of box girders in PT bridges

the influence of these parameters on C_T and probabilistic models to predict the C_T.

Trejo et al. (2009b) reported that grout class is not a critical parameter influencing C_T, when other exposure conditions remain the same. Therefore, grout class need not be considered for modeling C_T. Trejo et al. (2009a,b) identified five void conditions based on the geometry of the grout-air-strand interface at void locations and experimentally studied their effects on C_T. Fig. 2 shows the schematics of the test specimens used that represent the identified void conditions, which were defined as follows.

1. No void. This corresponds to the condition when the tendons are fully grouted and contain no significant voids. The 300-mm- (12-in.-) long strand surface beneath the reservoir [shown as "R" in Fig. 2(a)] has a 6-mm (0.25-in.) grout cover.
2. Parallel void. This corresponds to the condition when the strand is partially embedded in the grout and its longitudinal axis is parallel to the grout surface. This void condition may be found in tendon regions with a horizontal profile.
3. Bleed-water void. This corresponds to the condition when a thin layer of grout (typically formed due to the evaporation of bleed water) is present on the strand surface and the angle between the longitudinal axis of the strand and the grout surface is neither parallel nor orthogonal. In the test specimens in Fig. 2(c), the longitudinal axis of the partially embedded strand is at a 45° angle with the grout surface. This void condition may be found near anchorage zones of PT girders with an inclined tendon profile.
4. Inclined void. This corresponds to the condition that is similar to the bleed-water void condition, except that no thin layer of grout is present on the strand surface.
5. Orthogonal void. This corresponds to the condition when the strand is partially embedded in the grout and its longitudinal axis is orthogonal to the grout surface. This void condition may occur in PT columns or piers or other elements with a vertical profile. Depending on the flow characteristics of the fresh grout and the complex flow paths (due to the presence of convoluted strands inside the ducts) for the fresh grout, the orthogonal void type may also be found in PT ducts with horizontal or inclined profiles.

Based on these experimental data, Gardoni et al. (2009) developed probabilistic models to predict the C_T of unstressed strands exposed to the five void conditions mentioned earlier. However, strands on PT bridges experience a high axial stress of approximately $1,030\ \mathrm{N/mm^2}$ (150 ksi). The high axial stress can have a significant influence on strand corrosion and C_T. Proverbio and Longo (2003), Kovač et al. (2007), and Sanchez et al. (2007) reported that the synergistic effect of high stress levels and corrosive mediums can influence corrosion susceptibility, especially stress-corrosion cracking of prestressing strands. Also, Kovač et

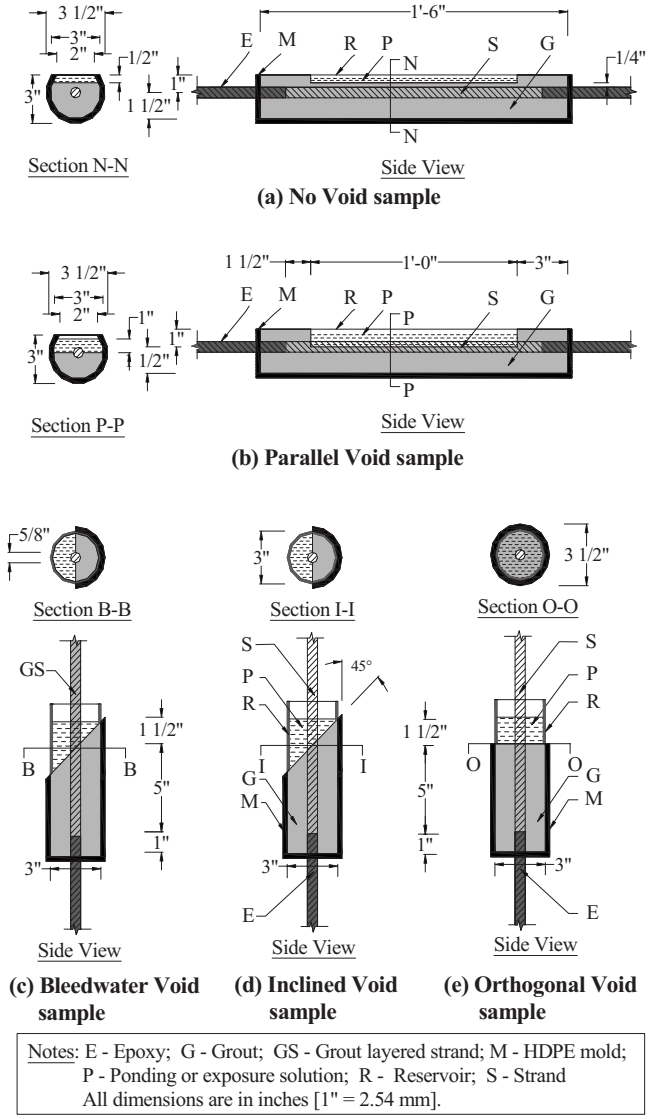

Fig. 2. Schematics of strand test samples [after Gardoni et al. (2009)]

al. (2007) reported the presence of transgranular cracks (with typical crack length equal to approximately 0.1 mm [0.004 in.]) on a cold-rolled prestressing steel subjected to stress levels corresponding to approximately 60% of its ultimate strength. In addition, Vu et al. (2009) reported that stress-corrosion-induced microcracks can result in a 25% reduction in elastic modulus and 15% reduction in the elastic limit before the brittle failure of wires. Trejo et al. (2009b) observed that the loss in C_T of stressed strands could be as high as 27% more than the loss of C_T of unstressed strands. These studies indicate that the corrosion and C_T loss of stressed strands are more than that of unstressed strands. Therefore, the C_T predicted using the models for unstressed strands developed by Gardoni et al. (2009) may be unconservative for field applications; indicating the need for new probabilistic models to predict the C_T of stressed strands in the field. In addition, Trejo et al. (2009b) found that bleed-water, inclined, and orthogonal voids cause statistically similar losses in C_T. Therefore, the data from the strand specimens with these void conditions are merged and one probabilistic model each is developed for the C_T of unstressed and stressed strands. The C_T of unstressed and stressed strands are denoted as $C_{T,\mathrm{US}}$ and $C_{T,\mathrm{SS}}$, respectively.

Table 1. Number of Test Specimens in the Experiment (the Numbers before and after Commas Correspond to Unstressed and Stressed Samples, Respectively); a Total of 24 As-Received Strand Specimens Were Also Tested

Exposure time, t (months)	Chloride ion concentration (%sCl$^-$)	Void type		
		No void	Parallel void	Bleed-water, inclined, or orthogonal void
12	0.0001[a]	10, 0	10, 0	30, 2
	0.006	10, 6	10, 6	30, 6
	0.018	10, 0	10, 0	30, 0
	0.18	10, 6	10, 6	20, 0
	1.8	10, 6	8, 6	28, 6
16	0.0001[a]	—	—	0, 2
	0.006	—	0, 6	0, 6
	0.18	—	0, 6	0, 6
	1.8	—	0, 6	0, 6
21	0.0001[a]	10, 0	10, 0	30, 2
	0.006	10, 6	10, 8	30, 8
	0.018	10, 0	10, 8	30, 8
	0.18	10, 6	10, 0	20, 0
	1.8	10, 6	9, 8	29, 8

[a]Control specimens exposed to standard room conditions without wet-dry cycles.

The remainder of this paper is organized as follows. First, the experimental program and test parameters are presented. Then, an overview of the probabilistic modeling of C_T and the analytical approach used to develop the models for stressed strands is presented. Then probabilistic models for unstressed and stressed strands are formulated. Then the parameters in these probabilistic models are assessed using a Bayesian approach. Practical applications of the developed models for stressed strands are then discussed prior to the section on conclusions.

Experimental Program and Test Parameters

This study used 15-mm- (0.6-in.-) diameter, low relaxation, seven-wire strands meeting the requirements of ASTM (2006) specifications. The mean and standard deviation of the C_T of the uncorroded strands used in the experiments are 264 kN (59.3 kips) and 1.3 kN (0.29 kips), respectively. Per the manufacturer, the elastic modulus of the strand was 1.93×10^5 N/mm^2 (2.8×10^4 ksi). A total of 374 unstressed and 162 stressed strand specimens were tested. These test specimens (see Fig. 2) were made of 1,040-mm- (41-in.-) long strand pieces that were completely or partially embedded in cementitious grout to represent the five void conditions. The fabricated test specimens were then exposed to wet-dry cycles (2-week ponding followed by 2-week drying) for different exposure times t. During the 2-week ponding period, the specimens were exposed to solutions containing different chloride concentrations (%sCl$^-$). Control specimens were also tested at standard room conditions (that is, 50–70% relative humidity and 21–29°C [70–85°F]) without wet-dry cycles. For the stressed strand specimens, a typical in-service stress level of 1,060 N/mm^2 (150 ksi) was maintained during the entire exposure period. Table 1 provides the number of unstressed and stressed strand specimens corresponding to each combination of void condition, %sCl$^-$, and t. The residual C_T of each strand specimen was determined at the end of the corresponding exposure time t. Note that losses in the cross-sectional area and weight of strand samples were not measured during the experiments. A brief description of test parameters used in this study is provided next.

Moisture or water at the metal surface is an essential component for the electrochemical process of steel embedded in cementitious materials (ACI 2003). The corrosion rate can increase when the chloride concentration at the strand surfaces increases and exceeds the critical chloride threshold level. Table 1 shows that the strand specimens were exposed to 0.0001, 0.006, 0.018, 0.18, and 1.8 %sCl$^-$ solutions. A concentration of 0.0001 %sCl$^-$ was assigned when the strands were in as-received conditions or not exposed to wet-dry cycles. Trejo et al. (2009a,b) and Pillai (2009) provided further details on the unstressed and stressed strand test programs.

General Approach for Probabilistic Modeling of Tension Capacity of Stressed Strands

In this paper, three models each to predict $C_{T,US}$ and $C_{T,SS}$ when the strands are exposed to three void conditions (i.e., no void, parallel void, and bleed-water, inclined, or orthogonal void conditions) are developed. The data from bleed-water, inclined, and orthogonal voids are grouped together because Trejo et al. (2009b) found that these voids cause statistically similar losses in C_T. Because PT strands in the field experience high axial stresses, the models for unstressed strands are not recommended for field applications; they are developed only to facilitate the development of the models for stressed strands. One approach in developing the models for $C_{T,SS}$ is based on regression using the experimental data from stressed strand samples only. However, the following approach is adopted to develop the models for $C_{T,SS}$ in this paper. This approach allows updating the models when additional data from the less expensive unstressed strand testing become available.

At first, diagnostic plots are developed to identify the appropriate explanatory functions for $C_{T,US}$. Then, based on the underlying corrosion principles and visible trends in the diagnostic plots, the models for unstressed strands are formulated. These models are then assessed using the data from unstressed strand samples exposed for t=0, 12, and 21 months. For each observed value of $C_{T,SS}$, the median of $C_{T,US}$ is predicted using the models for unstressed strands. The relationship between observed values of $C_{T,SS}$ and corresponding median of $C_{T,US}$ are diagnosed, and the models for stressed strands are formulated. The formulated models for stressed strands are then assessed using the data on $C_{T,SS}$ (i.e., the data observed at 0, 12, 16, and 21 months of exposure) and corresponding median value of $C_{T,US}$.

Following the general formulation of probabilistic models in Gardoni et al. (2002b), the $C_{T,US}$ and $C_{T,SS}$ are formulated as follows:

$$R_C(\mathbf{x},\boldsymbol{\Theta}) = \gamma(\mathbf{x},\boldsymbol{\theta}) + \sigma\varepsilon \quad (1)$$

where $R_C(\mathbf{x},\boldsymbol{\Theta})$=ratio between the C_T and MUTS; $\gamma(\mathbf{x},\boldsymbol{\theta})$=correction function; $\mathbf{x}$=vector of the basic explanatory variables or regressors; $\boldsymbol{\Theta}=(\boldsymbol{\theta},\sigma)$=vector of unknown model parameters, where $\boldsymbol{\theta}=(\theta_1,\ldots,\theta_k)=1\times k$ vector of model parameters; and $\sigma\varepsilon$=model error, where σ=standard deviation of model error and ε=normal random variable [$\sim N(0,1)$].

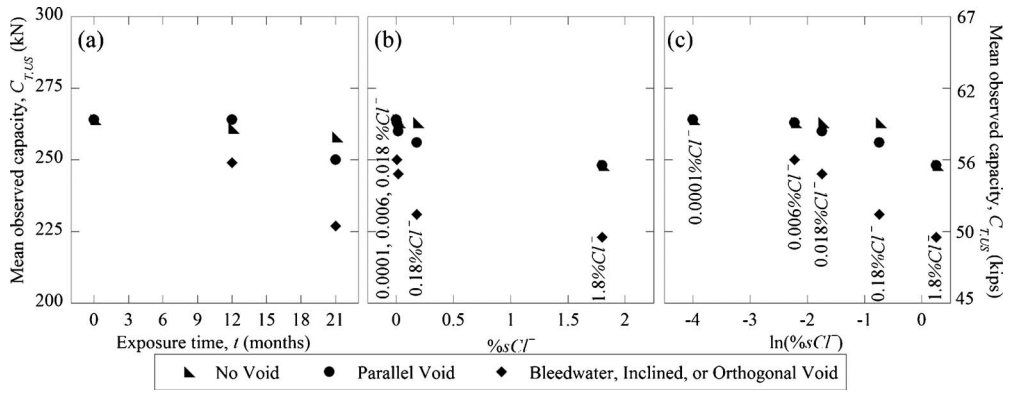

Fig. 3. Effect of time and chloride functions on mean $C_{T,US}$, when exposed to various void conditions

In the models developed in this paper, the basic response and explanatory functions (with the exception of explanatory functions based on t) are standardized to form dimensionless explanatory functions. To simplify the model expressions, these modified or standardized explanatory functions are denoted using the letter h with a subscript representing the corresponding basic explanatory variable x. In other words, the term x represents the data collected from the experiments and the term h in the models is a function of x. Models with dimensionless response and explanatory functions have the following two benefits over those made of parameters with specific physical dimensions: (1) The vector $\boldsymbol{\theta}$ associated with dimensionless parameters is also dimensionless, and (2) a dimensionless model is applicable when the standardized explanatory functions fall within the range of the standardized explanatory functions in the database used to develop the model. This approach typically expands the range of applicability of a probabilistic model.

Formulation of Probabilistic Models for Unstressed and Stressed Strands

Based on diagnostic studies, this section formulates the models for unstressed and stressed strands. At first, three models for unstressed strands are formulated. Then the three corresponding models for stressed strands are formulated.

Formulation of Models for Unstressed Strands

The probabilistic models for unstressed strands are formulated in this section. Fig. 3 provides diagnostic plots on the effects of t, $\%s\mathrm{Cl}^-$, and $\ln[\%s\mathrm{Cl}^-]$ on $C_{T,US}$. Only the mean values of the observed data associated with each void condition are shown in these figures. Each data marker in Fig. 3(a) indicates the mean $C_{T,US}$ observed among the samples exposed to all chloride levels and at a particular exposure time. Similarly, each data marker in Figs. 3(b and c) indicates the mean $C_{T,US}$ observed among the samples exposed to all exposure times and at a particular chloride level. Trejo et al. (2009a) provided the scatter plots with all the data points.

Main Effect of Time Parameter

Many researchers have modeled corrosion of metallic materials as a time-dependent process. For example, Akgül and Frangopol (2004) assumed a linear time function [i.e., 0.0572 mm/year (2.25 mils/year)] for corrosion of pretensioned strands in concrete. Also, the graphical representations in Melchers (2003) suggest that a linear corrosion loss assumption is reasonable for long-term immersion corrosion of alloy steels. The experimental data from this study also indicate similar behavior. Fig. 3(a) indicates a reasonably good linear relationship between the mean $C_{T,US}$ and t. In the cases of samples with no void (triangular markers) and bleed-water, inclined, or orthogonal void conditions (diamond markers), the linear relationship is reasonable. For the parallel void condition (circular markers), the rate of loss of $C_{T,US}$ is minimal until 12 months, after which this rate increases. In strand corrosion, the cathode-anode ratio influences the rate of corrosion in a local region (i.e., anode) on the strand. The rate of localized corrosion influences the rate of reduction in tension capacity. On parallel void samples, one side of a 12-in. portion of the strand was exposed to chloride solution [see Fig. 2(b)] resulting in a cathode-anode ratio of 0.5, which was insufficient to cause significant loss in tension capacity within 12 months. However, the cathode-anode ratios on bleed-water, inclined, and orthogonal void samples [see Figs. 2(c–e)] were approximately 5, which resulted in a more severe localized corrosion and faster reduction in the tension capacity within 12 months. In the case of no void samples [see Fig. 2(a)], the cathode-anode ratio was unknown. However, the chlorides from the exposure solution could penetrate through the cracks in the grout cover and form corrosion cells on the embedded strand surface. These corrosion cells could have had high cathode-anode ratio resulting in a significant reduction in the tension capacity within 12 months. A linear relationship for parallel voids is weaker than those observed for no void (triangular markers) and bleed-water, inclined, or orthogonal void conditions (diamond markers). However, in an effort to keep similar model forms for all void conditions, a function linear on t is considered to construct all the models for unstressed strands.

In the field, water may infiltrate the tendons and keep it wet (e.g., standing water has been observed in the tendons of PT bridges in Florida). This water could dry out through natural drying process. However, the wet time could be different for different bridge locations. The rate of strand corrosion during the wet time may be higher than that during the dry time. Therefore, the total wet time h_t is more critical than the total exposure time t for calculating time-variant tension capacity of strands. The term h_t is calculated as follows:

$$h_t = \phi_{wet} \times t = \left(\frac{\text{average wet time in 1 year(months)}}{12\text{(months)}} \right) \times t\text{(years)} \quad (2)$$

where ϕ_{wet}=wet-factor representing the severity of wet-dry condition and can be calculated using the number of wet or rainy days. In the laboratory experiments, the wet-dry cycles (2-week wet followed by a 2-week dry) correspond to a wet time of 6 months in every 12 months and, therefore, correspond to a ϕ_{wet} of 0.5 [obtained by dividing the wet time in 1 year (i.e., 6 months) by 12 months]. The value of ϕ_{wet} can be changed by the user depending on the actual or expected wet-dry conditions inside the tendons in the field. Further details on the calculation of ϕ_{wet} are provided later.

Two-Way Interaction Effect of Chloride and Time Parameters

The main effect of $\%s\text{Cl}^-$ on $C_{T,US}$ is diagnosed first. Fig. 3(b) shows the scatter plot between the mean $C_{T,US}$ and $\%s\text{Cl}^-$. The vertical text near the data markers indicates the actual $\%s\text{Cl}^-$ values corresponding to the data markers. When no void conditions (triangular data markers) exist, the relationship between the mean $C_{T,US}$ and $\%s\text{Cl}^-$ seems approximately linear. However, the circular and diamond markers indicate that a linear relationship between the mean $C_{T,US}$ and $\%s\text{Cl}^-$ is inappropriate when parallel void and bleed-water, inclined, or orthogonal void conditions, respectively, exist.

Fig. 3(c) shows the relationship between the mean $C_{T,US}$ and natural logarithm of $\%s\text{Cl}^-$ (i.e., $\ln[\%s\text{Cl}^-]$). The vertical text near the data markers indicates the actual $\%s\text{Cl}^-$ values corresponding to the $\ln[\%s\text{Cl}^-]$ values on the abscissa. The circular and diamond markers in Fig. 3(c) indicate that linear relationship between the mean $C_{T,US}$ and $\ln[\%s\text{Cl}^-]$ is reasonable, when parallel void and bleed-water, inclined, or orthogonal void conditions, respectively, exist. In addition, when the no void condition (triangular markers) exists, the reduction in capacity is negligible until $\%s\text{Cl}^-$ reaches 0.18 and significantly increases when $\%s\text{Cl}^-$ is 1.8. This is probably due to the following behavior. In the case of samples exposed to 0, 0.018, and 0.18 $\%s\text{Cl}^-$ solutions, there was not sufficient time for the chloride ions to travel (i.e., via diffusion) through the 6-mm (0.25-in.) grout cover and reach the steel surface to initiate chloride-induced corrosion. However, in the case of samples exposed to 1.8 $\%s\text{Cl}^-$ solution, high amounts of chloride ions were deposited in the microcracks in the grout cover and traveled toward the steel surface at a faster rate (i.e., via sorption and/or diffusion). The data indicate that $\ln[\%s\text{Cl}^-]$ is not an appropriate explanatory function for the no void condition. Based on Figs. 3(b and c) and the above discussion, explanatory function $h_{s\text{Cl}^-}$ is selected as follows:

$$h_{s\text{Cl}^-} = \begin{cases} \dfrac{\%s\text{Cl}^-}{\%s\text{Cl}^-_{\text{saturated chloride solution}}} = \dfrac{\%s\text{Cl}^-}{35.7} & \text{for no void conditions} \\ \ln\left(\dfrac{\%s\text{Cl}^-}{\%s\text{Cl}^-_{\text{saturated chloride solution}}} \right) = \ln\left(\dfrac{\%s\text{Cl}^-}{35.7} \right) & \text{for parallel, bleed-water, inclined, and orthogonal void conditions} \end{cases} \quad (3)$$

However, from an electrochemical point of view, $h_{s\text{Cl}^-}$ has no main effect on $C_{T,US}$, especially when the probabilistic models are developed to predict both short- and long-term performances. This reasoning can be justified as follows. A high value of t and 0 $\%s\text{Cl}^-$ (e.g., no exposure to chloride solution for 100 years) or a high value of $\%s\text{Cl}^-$ and zero t (e.g., seawater for 1 day) do not normally lead to significant corrosion and reduction in C_T. Therefore, the two-way interaction term $h_{s\text{Cl}^-}h_t$ is anticipated to be a better explanatory function than $h_{s\text{Cl}^-}$. From a statistical standpoint, the interaction term helps satisfy the homoskedasticity assumption. The homoskedasticity assumption means that σ is approximately constant and independent of the explanatory functions. The normality assumption means that ε follows a normal distribution.

Probabilistic Model Forms

Based on the diagnostic studies, the models for unstressed strands are formulated as follows:

$$R_{C_{T,US}}(\mathbf{x}, \boldsymbol{\Theta}_{US}) = \underbrace{\theta_{US,0} + \theta_{US,1}h_t + \theta_{US,2}h_{s\text{Cl}^-}h_t}_{\gamma(\mathbf{x}, \boldsymbol{\theta}_{US})} + \sigma_{US}\varepsilon \quad (4)$$

where the terms are as defined in Eqs. (1)–(3). The MUTS of an as-received strand is 264 kN (58.6 kips) and the observed median of $C_{T,US}$ was 261 kN (59.3 kips), which is slightly larger than its MUTS. Therefore, when t is zero, the model should predict a $C_{T,US}$ that is slightly larger than its MUTS. The intercept term will help meet this criterion. The term $h_{s\text{Cl}^-}h_t$ will capture the effect of interaction between the chloride and time.

Formulation of Models for Stressed Strands

This section formulates the probabilistic models to predict $C_{T,SS}$.

Relationship between the Capacities of Unstressed and Stressed Strands

As discussed earlier, the observed $C_{T,SS}$ data from the stressed strand testing and the corresponding values of the medians of $C_{T,US}$ obtained using the models for unstressed strands are used to develop the models for stressed strands. Fig. 4 shows the scatter plots between the predicted median of $C_{T,US}$ and observed values of $C_{T,SS}$. The predicted median of $C_{T,US}$ is shown on the abscissa because it is an explanatory variable for the model for $C_{T,SS}$. The observed values of $C_{T,SS}$ are shown on ordinate. At first, it might seem that a linear relationship between $C_{T,US}$ and $C_{T,SS}$ exists. However, preliminary analysis indicated that a linear model tends to overestimate the value of $C_{T,SS}$, when it is near MUTS. Hence, a power model is used.

Probabilistic Model Form

Following a power model form, the models for stressed strands will be formulated as follows:

$$R_{C_{T,SS}}(\mathbf{x}, \boldsymbol{\Theta}_{SS}) = \theta_{SS,0}[\gamma(\mathbf{x}, \boldsymbol{\theta}_{US})]^{\theta_{SS,1}} + \sigma_{SS}\varepsilon \quad (5)$$

where the terms are as defined in Eqs. (1) and (4). The power model form in Eq. (5) does not have an intercept term and, there-

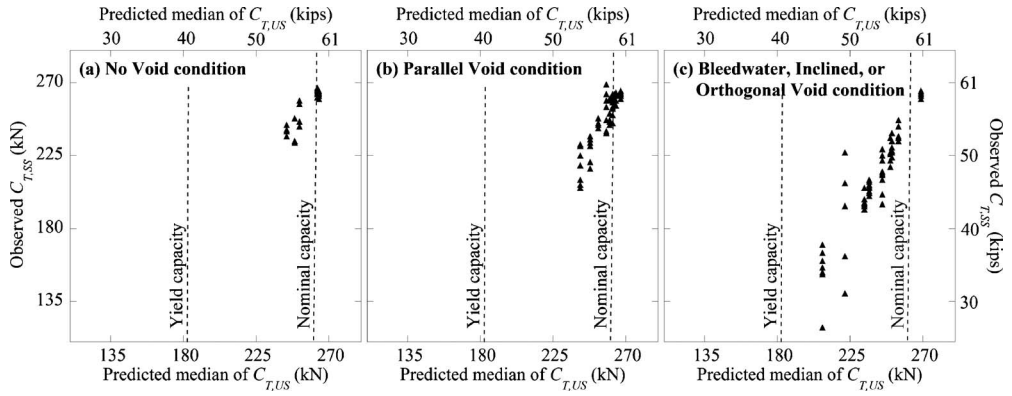

Fig. 4. Scatter plots between median values of $C_{T,US}$ and observed values $C_{T,SS}$

fore, ensures that $C_{T,SS}$ is zero when $C_{T,US}$ is zero.

Assessment of Probabilistic Models for Unstressed and Stressed Strands

For the models for unstressed strands, the model form is linear in its parameters, no prior information is available for the distribution of $\boldsymbol{\Theta}_{US}$, and no upper or lower bounds of the data are used. Therefore, Bayesian closed-form solution procedures (Box and Tiao 1992) can be used to assess the posterior statistics of $\boldsymbol{\Theta}_{US}$. For the models for stressed strands, the model form is nonlinear in its parameters, no prior information is available about the distribution of $\boldsymbol{\Theta}_{SS}$, and the upper and lower bounds of the data are undefined. Therefore, an importance sampling technique (Gardoni et al. 2002a) is used to assess the posterior statistics of the models for stressed strands. The term σ_{SS} is a measure of model accuracy. In addition to σ_{SS}, the mean absolute percentage error (MAPE) is used to provide a more intuitive measure of model accuracy. The MAPE is the average error in the model expressed as a percent of the observed value and is mathematically expressed as follows:

$$\text{MAPE} = \frac{1}{n}\sum_{i=1}^{n}\left(\frac{|\text{median}[C_T(\mathbf{x}_i,\boldsymbol{\theta})] - C_{T,i}|}{C_{T,i}}\right) \times 100 \qquad (6)$$

where n=number of observations; $C_{T,i}$=ith observed value of C_T; and $C_T(\mathbf{x}_i,\boldsymbol{\theta})$=$C_T$ obtained using the developed models.

Assessment of Models for Unstressed Strands

The models for unstressed strands in Eq. (4) are assessed using a Bayesian approach and the data from the 0-, 12-, and 21-month-long unstressed strand corrosion testing. Table 2 summarizes the MAPE and posterior statistics of model parameters. Fig. 5 shows the scatter plots between the observed (shown in abscissa) and median predicted (shown in ordinate) values of $C_{T,US}$. For a per-

Table 2. MAPE and Posterior Statistics of the Models for Unstressed and Stressed Strands under Various Void Types

Model identification		MAPE (%)	Model parameters	Mean	Standard deviation	COV	Correlation coefficients between θ_i		
							θ_0	θ_1	θ_2
Models for unstressed strands	No void	1.2	$\theta_{US,0}$	1.0105	0.0022	0.002	1		
			$\theta_{US,2}$	–1.6785	0.1362	–0.08	−0.47		1
			σ_{US}	0.0194	0.0073	0.38			
	Parallel void	1.6	$\theta_{US,0}$	1.0232	0.0047	0.005	1		
			$\theta_{US,1}$	–0.1553	0.0141	–0.09	−0.45	1	
			$\theta_{US,2}$	–0.0153	0.0019	–0.12	0.01	0.84	1
			σ_{US}	0.0256	0.0098	0.38			
	Bleed-water, inclined, or orthogonal void	3.2	$\theta_{US,0}$	1.0333	0.0056	0.005	1		
			$\theta_{US,1}$	–0.3567	0.0124	–0.03	−0.61	1	
			$\theta_{US,2}$	–0.0285	0.0015	–0.05	0.01	0.74	1
			σ_{US}	0.0350	0.0107	0.31			
Models for stressed strands	No void	0.7	$\theta_{SS,0}$	0.9983	0.0014	0.001	1		
			$\theta_{SS,1}$	1.3576	0.0648	0.05	0.04	1	
			σ_{SS}	0.0117	0.0011	0.09			
	Parallel void	1.9	$\theta_{SS,0}$	0.9748	0.0028	0.003	1		
			$\theta_{SS,1}$	1.8139	0.1009	0.06	0.14	1	
			σ_{SS}	0.0244	0.0020	0.08			
	Bleed-water, inclined, or orthogonal void	3.2	$\theta_{SS,0}$	0.9463	0.0064	0.007	1		
			$\theta_{SS,1}$	2.0301	0.0773	0.04	0.47	1	
			σ_{SS}	0.0411	0.0034	0.08			

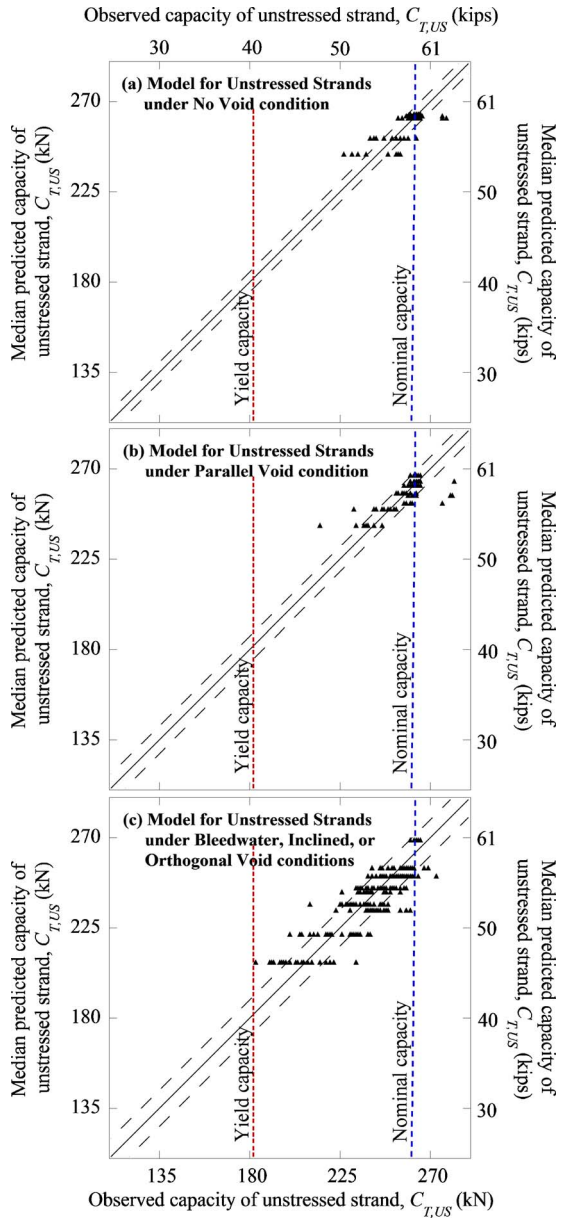

Fig. 5. Validation plots for the models for unstressed strands

fect prediction model, the predicted and observed capacities would line up along the 1:1 solid lines. However, due to potential variations in the actual exposure conditions and the observed values of $C_{T,US}$, possible measurement errors, and possible model errors due to missing variables in Eq. (1) or an inaccurate model form in Eq. (4), there is a scatter around the 1:1 line. In particular, different values of $C_{T,US}$ are observed from strand samples with identical combinations of test parameters. The two dashed lines in the validation plots delimit the region within one standard deviation from the 1:1 line. Following is a discussion on the assessment of the models for unstressed strands exposed to various void conditions.

Model for Unstressed Strands Exposed to No Voids

The MAPE and posterior statistics of the model form for the no void condition were assessed using the data from the unstressed strands with no void conditions. Following the model selection process in Gardoni et al. (2002b), it is found that the coefficient of variation (COV) of θ_1 (corresponding to h_t) is high (i.e., 1.77) when compared to the estimate of σ_{US}. Therefore, h_t is removed from the full model to form a reduced model. Table 2 provides the MAPE and posterior statistics of the reduced model. The coefficients (i.e., $\theta_{US,0}$ and $\theta_{US,2}$) of the explanatory functions have reasonably small COVs (i.e., 0.002 and −0.08, respectively). Also, the MAPE and σ_{US} are reasonably small (i.e., 1.2% and 0.0194, respectively). These observations indicate good prediction accuracies for the reduced model. The reduced model is the most parsimonious model with reasonable accuracy. This also indicates that only the intercept and the two-way interaction term (i.e., h_{sCl}-h_t) are needed to predict $C_{T,US}$ when the tendons are fully grouted. This is supported by the fact that if the chloride exposure level is low, it takes a long time for the available chloride ions to be transported through the 6-mm- (0.25-in.-) thick grout cover [see Fig. 2(a)], reach the strands in sufficient quantity, and initiate corrosion. Testing with exposure periods longer than 21 months would likely have provided sufficient data to observe chloride-induced corrosion, especially when the $\%sCl^-$ level of the test solution was 0.006 or 0.018. However, such a longer-term testing was beyond the scope of this research. The test specimens exposed to 0.18 and 1.8 $\%sCl^-$ exhibited relatively larger reductions in capacity. Fig. 5(a) shows the validation plot for the model for the no void condition.

Model for Unstressed Strands Exposed to Parallel Voids

The MAPE and posterior statistics of the model form for the parallel void condition are assessed using the data from the unstressed strand specimens exposed to a parallel void condition. Table 2 shows that the model parameters (i.e., $\theta_{US,0}$, $\theta_{US,1}$, and $\theta_{US,2}$) have small COVs (i.e., 0.005, −0.09, and −0.12, respectively), indicating good confidence in the mean parameter estimations. These parameters indicate that $C_{T,US}$, when exposed to parallel void condition, is more sensitive to h_t than h_{sCl}-h_t; however, this data-based conclusion is specific to the data analyzed and could change as more data are available. This model also exhibits a reasonably small MAPE and σ_{US} (i.e., 1.6% and 0.0256), indicating good model accuracy. Fig. 5(b) shows the validation plot for the model for parallel void condition. Among the 77 data points, the 4 data points near the top right region show underestimation and the 2 data points near the bottom left region show overestimation of $C_{T,US}$. Most of the remaining data points fall along the 1:1 line (spread with an approximately equal width) and exhibit no significant bias or residual trend. The spread of most data points along the 1:1 line indicates good prediction accuracy.

Model for Unstressed Strands Exposed to Bleed-Water, Inclined, or Orthogonal Voids

Table 2 shows that the MAPE and σ_{US} for the model for bleedwater, inclined, or orthogonal voids are reasonably small (i.e., 3.2% and 0.0350, respectively). The mean estimates for $\theta_{US,1}$ and $\theta_{US,2}$ indicate that the capacity is more sensitive to the changes in h_t than those to h_{sCl}-h_t; however, this data-based conclusion is specific to the data analyzed and could change as more data are available. The COVs of the model parameters $\theta_{US,0}$, $\theta_{US,1}$, and $\theta_{US,2}$ are 0.005, −0.03, −0.05, respectively. These observations and validation plot in Fig. 5(c) exhibit reasonably good prediction accuracy. As shown in Fig. 5(c), although variability exists among the observed $C_{T,US}$ for identical exposure conditions, the mean of the observed values of $C_{T,US}$ corresponding to a particular predicted $C_{T,US}$ lies close to the 1:1 line. This indicates good accu-

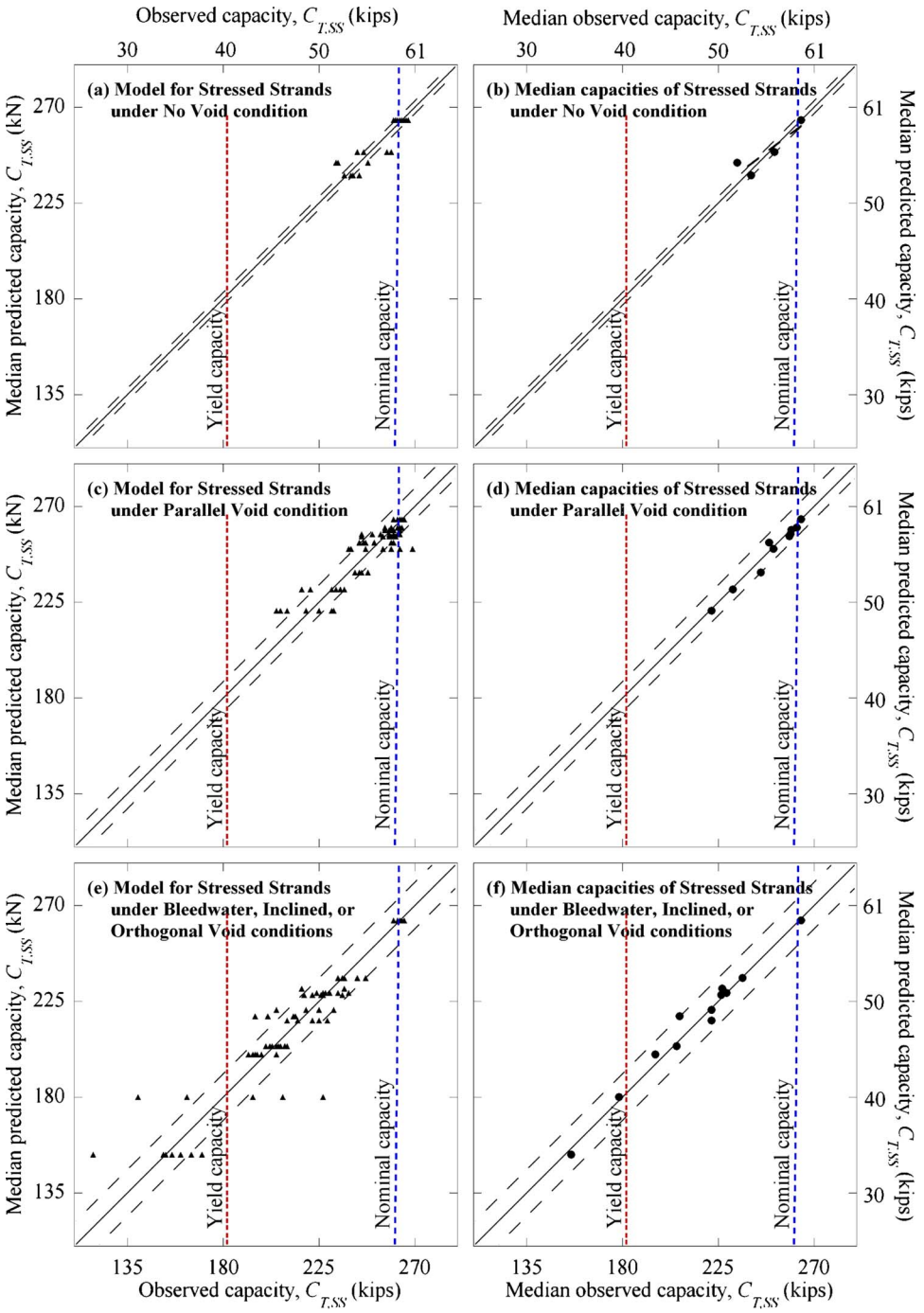

Fig. 6. Validation plots for the models for stressed strands

racy in model prediction, given the inherent variability (due to the unknown variations in the exposure conditions and strand characteristics) in the corrosion process.

Assessment of Models for Stressed Strands

This section presents the assessment of the models to predict $C_{T,SS}$. These models are assessed using the $C_{T,SS}$ data obtained from the 0-, 12-, 16-, and 21-month-long stressed strand testing and corresponding median values of $C_{T,US}$. The median values of $C_{T,US}$ are determined using the models for unstressed strands. Following is the description of the assessment of the models for stressed strands exposed to various void conditions.

Model for Stressed Strands Exposed to No Voids

This model can be used to predict $C_{T,SS}$ when the strands are completely embedded inside a cementitious grout. Table 2 shows that the COVs of $\theta_{SS,0}$ and $\theta_{SS,1}$ are 0.001 and 0.05, indicating good confidence in their mean estimates. Also, the mean and COV of σ_{SS} are 0.0117 and 0.09, respectively. These results indicate that the model can reasonably predict $C_{T,SS}$ with reasonable accuracy. In addition, the MAPE of this model for the no void condition is 0.7%. The data in Fig. 6(a) are spread along the 1:1 line and do not show any significant residual trend. Also, the scatter plot between the median observed and median predicted values shown in Fig. 6(b) indicates reasonably good prediction.

Model for Stressed Strands Exposed to Parallel Voids

This model can be used to predict the $C_{T,SS}$ when voids exist near the midspan regions in tendons. This model is not appropriate to predict the $C_{T,SS}$ when voids exist near the anchorages with inclined or vertical profiles. Table 2 shows that the MAPE and σ_{SS} for this model are reasonably small (i.e., 1.9% and 0.0244). In addition, the COVs of the model parameters $\theta_{SS,0}$ and $\theta_{SS,1}$ are 0.003 and 0.06, respectively; indicating good confidence in their mean estimates. Fig. 6(c) shows the validation plot for this model, with the data falling near the 1:1 line and no significant residual trend pattern. In addition, a reasonably good prediction is exhibited by the scatter plot between the median observed and median predicted values of $C_{T,SS}$ [see Fig. 6(d)].

Model for Stressed Strands Exposed to Bleed-Water, Inclined, or Orthogonal Voids

The bleed-water, inclined, and orthogonal voids are possibly the most prevalent void conditions found on PT systems in bridges (Schupack 2004). The model in this subsection can be used to predict $C_{T,SS}$ when voids exist at or near the anchorage regions of PT columns or girders. The power model form in Eq. (5) was assessed using the data from the stressed strands exposed to bleed-water, inclined, and orthogonal void conditions and the corresponding median values of $C_{T,US}$ predicted using the corresponding model for unstressed strands. Table 2 shows the MAPE and posterior statistics of this model. The MAPE and σ_{SS} are reasonably small (i.e., 3.2% and 0.0411, respectively). The high confidence levels on the mean estimates of the model parameters (i.e., $\theta_{SS,0}$ and $\theta_{SS,1}$) are demonstrated by their small COVs (i.e., 0.007 and 0.04, respectively). The validation plot for the model [Fig. 6(e)] indicates good prediction accuracy and no significant trend in the residuals from their median values. Also, the scatter plot between the median observed and median predicted values shown in Fig. 6(f) indicates reasonably good prediction. Because of these reasons, it can be concluded that the model is reasonably homoskedastic. However, a large scatter is observed among the five data points corresponding to the predicted capacity of approximately 178 kN (40 kips). This large scatter is probably not due to the model inadequacy, rather is due to the inherent scatter in the observed values of $C_{T,SS}$ under identical exposure conditions.

Practical Applications of Probabilistic Models for Stressed Strands

The models developed for unstressed strands should not be used for field applications. The models developed for stressed strands can be used for predicting the C_T of stressed strands in PT bridges when various void, moisture, and chloride conditions exist. The strands used in this study are similar to the strands used in practice. Therefore, the probabilistic models developed in this document should be applicable to the strands in practice. These models can also be used to predict the C_T of strands with other diameters, provided its MUTS is used. An example of the prediction of $C_{T,SS}$ using the developed models for stressed strands is provided next.

To use these models for predicting the C_T of tendons in PT bridges, an appropriate value of ϕ_{wet} (i.e., the factor defining the severity of wet-dry exposure) inside the tendons has to be obtained. In the following example, ϕ_{wet} is assumed based on the precipitation data obtained from NCDC (2008) and the following three definitions: (1) *time to dry*: the time required for the grout inside of tendons to dry (i.e., through self-desiccation and the natural drying process), (2) *rain day*: a day with precipitation, and (3) *wet day*: either a rain day or a day with at least one rain day within a period of time to dry prior to the day under consideration. Based on the NCDC (2008) precipitation data for the downtown region in San Antonio, Tex. for the years 2001, 2002, 2003, 2004, and 2005 and the above definitions, the average number of wet days for assumed time to dry values of 1, 2, 3, 4, 5, 6, and 7 weeks ranges from 69 to 82 days [details are provided by Pillai (2009)]. The corresponding values of ϕ_{wet} are 0.19 and 0.22 (i.e., 2.3 and 2.6 months of wet time in 1 year, respectively). For all the capacity predictions provided in the remainder of this section, ϕ_{wet} is assumed to be 0.17 (i.e., 2 months of wet time in 1 year).

Fig. 7 shows the predicted values of $C_{T,SS}$ under various exposure conditions and provides a comparison with the nominal capacity (i.e., MUTS) and yield capacity of strands. Figs. 7(a and

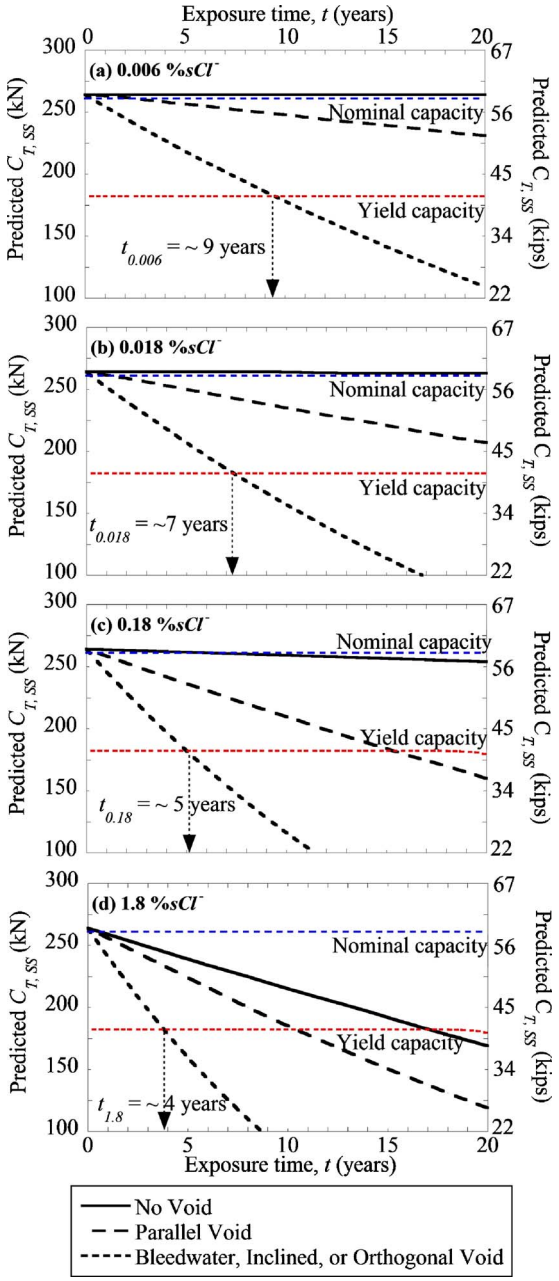

Fig. 7. Predicted capacities of stressed strands exposed to different chloride conditions with $\phi_{wet}=0.17$

b) show that negligible reduction in $C_{T,SS}$ may be expected when no void and 0.006 or 0.18 $\%s\text{Cl}^-$ conditions exist for 20 years. Figs. 7(c and d) show that, in the case of no void condition, the exposure to 0.18 and 1.8 $\%s\text{Cl}^-$ solutions (i.e., moderate and high chloride conditions) can cause $C_{T,SS}$ to reach below MUTS within 7 years and 1 year, respectively. Figs. 7(a–d) indicate that, for parallel void and bleed-water, inclined, or orthogonal void conditions, the predicted $C_{T,SS}$ can, in general, reach below MUTS within approximately 1 year. For samples exposed to parallel void and 0.006 $\%s\text{Cl}^-$ conditions, $C_{T,SS}$ dropped below MUTS within approximately 2 years.

For PT strands with a nominal ultimate tensile stress (f_{pu}) of $1,860\ \text{N/mm}^2$ (270 ksi), a typical effective stress due to service load conditions (f_{pe}) is $1,030\ \text{N/mm}^2$ (150 ksi). However, when computing the nominal flexural resistance (for loads above service levels), the AASHTO LRFD (2008) limits the estimated average stress in unbonded PT strands to not exceed the yield strength (f_{py}). For Grade 270 strands, f_{py} is $1,670\ \text{N/mm}^2$ (243 ksi). Because of the corrosion-induced reduction in the cross-sectional area of strands, the actual stresses on strands may also reach values above the typical service stress levels. The time to reach a reduced strand capacity corresponding to f_{py} could also be selected as a critical parameter for assessing the impact of corrosion. Figs. 7(a–d) show that when bleed-water, inclined, or orthogonal void and wet-dry conditions exist, $C_{T,SS}$ can reach a value below the yield capacity within approximately 9, 7, 5, and 4 years (shown by vertical arrows) when exposed to 0.006, 0.018, 0.18, and 1.8 $\%s\text{Cl}^-$ solutions, respectively. These time estimates are comparable to the time to tendon failures in the PT bridges in Florida and Virginia (i.e., 4–16 years).

Summary and Conclusions

A 21-month-long strand corrosion test program (with 384 unstressed and 162 stressed strand specimens) was conducted. Based on the data from unstressed strand testing, the models for unstressed strands were developed to estimate the capacity of 15-mm- (0.6-in.-) diameter, low relaxation, seven-wire strands meeting the ASTM A416 specifications and used in voided tendons with direct exposure to moisture and/or chlorides. Then, the capacity of unstressed strands predicted using these models and experimental data from 162 stressed strand specimens were correlated, and the models to predict the tension capacity of stressed strands in the field were developed. The MAPE values of these models were less than 3.2%, indicating good overall model accuracy. The strands inside fully grouted tendons (i.e., without voids) exhibited the lowest amount of corrosion and capacity reduction. The strands in grouted tendons with parallel voids exhibited slightly higher capacity reductions than those in fully grouted tendons. The strands in tendons with bleed-water, inclined, or orthogonal voids exhibited slightly higher capacity reductions than those in tendons with parallel voids. The time for strands to reach a reduced capacity corresponding to their yield strength was predicted using the developed models. These durations are comparable with the times to tendon failures observed in the bridges in Florida and Virginia.

Acknowledgments

This research was performed at the Texas Transportation Institute (TTI) and Zachry Department of Civil Engineering, Texas A&M University (TAMU), College Station, Tex., through a sponsored project from the Texas Department of Transportation (TxDOT), Austin, Tex. This support is much appreciated. The writers acknowledge the support from Keith Ramsey (Program Coordinator), Jaime Sanchez (Project Director I), Maxine Jacoby (Project Director II), German Claros (Project Director III), Brian Merrill (Project Director IV), Dean Van Landuyt, Kenneth Ozuna, Steve Strmiska, Tom Rummel, and other TxDOT engineers. The writers acknowledge Jeff Perry and Matt Potter of the High Bay Structural Materials Laboratory; Scott Crauneur of the Zachry Department of Civil Engineering; and Duane Wagner, Cheryl Burt, Scott Dobrovolny, Robert Kocman, and Gary Gerke of TTI for their assistance during the experimental phase of this research. The writers also acknowledge the assistance from Daren Cline, Ramesh Kumar, and Byoung Chan Jung during the analytical phase of this research.

References

AASHTO LRFD. (2008). *AASHTO LRFD bridge design specifications*, American Association of the State Highway and Transportation Officials, Washington, D.C.

ACI. (2003). "222R-03—Protection of metals in concrete against corrosion." *ACI Communication 222*, *Document No. 22203*, American Concrete Institute, Detroit.

Akgül, F., and Frangopol, D. M. (2004). "Lifetime performance analysis of existing prestressed concrete bridge superstructures." *J. Struct. Eng.*, 130(12), 1889–1903.

ASBI. (2000). *American Segmental Bridge Institute Grouting Committee: Interim statement on grouting practices*, American Segmental Bridge Institute, Phoenix.

ASTM. (2006). "Standard specification for steel strand, uncoated seven-wire for prestressed concrete." *ASTM A416*, West Conshohocken, Pa.

Box, G. E. P., and Tiao, G. C. (1992). *Bayesian inference in statistical analysis*, Addison-Wesley, Reading, Mass., 113–122.

FDOT. (2001a). "Mid-bay bridge post-tensioning evaluation—Final report." *Rep. Prepared for Corven Engineering, Inc.*, Florida Dept. of Transportation, Tallahassee, Fla.

FDOT. (2001b). "Sunshine skyway bridge post-tensioned tendons investigation." *Rep. Prepared for Parsons Brinckerhoff Quade and Douglas, Inc.*, Florida Dept. of Transportation, Tallahassee, Fla.

Gardoni, P., Der Kiureghian, A., and Mosalam, K. M. (2002b). "Probabilistic capacity models and fragility estimates for reinforced concrete columns based on experimental observations." *J. Eng. Mech.*, 128(10), 1024–1038.

Gardoni, P., Pillai, R. G., Hueste, M. D., Reinschmidt, K., and Trejo, D. (2009). "Probabilistic capacity models for corroding posttensioning strands calibrated using laboratory results." *J. Eng. Mech.*, 135(9), 906–916.

Gardoni, P. G., Der Kiureghian, A., and Mosalam, K. M. (2002a). "Probabilistic capacity models and fragility estimates for bridge components and systems." *PEER Rep. No. 2002/13*, Pacific Earthquake Engineering Research Center, Dept. of Civil Engineering, Univ. of California, Berkeley, Calif.

Kovač, J., Leban, M., and Legat, A. (2007). "Detection of SCC on prestressing steel wire by the simultaneous use of electrochemical noise and acoustic emission measurements." *Electrochim. Acta*, 52, 7607–7616.

Melchers, R. E. (2003). "Modeling of marine immersion corrosion for mild and low-alloy steels—Part 1: Phenomenological model." *Corrosion (Houston)*, 59(4), 319–334.

NCDC. (2008). "National Climatic Data Center (NCDC)." ⟨www.ncdc.noaa.gov⟩ (Nov. 1, 2008).

NCHRP. (1998). "Durability of precast segmental bridges." *NCHRP Web Document No. 15, Project 20–7/Task 92*, R. W. Poston and J. P. Wouters, eds., National Cooperative Highway Research Program,

Transportation Research Board, National Research Council, Washington, D.C.

Pillai, R. G. (2009). "Electrochemical characterization and time-variant structural reliability assessment of post-tensioned, segmental concrete bridges." Ph.D. thesis, Zachry Dept. of Civil Engineering, Texas A&M Univ., College Station, Tex.

Poston, W. R., Frank, K. H., and West, J. S. (2003). "Enduring strength." *Civil Engineering, American Society of Civil Engineering*, 73(9), 58–63.

Proverbio, E., and Longo, P. (2003). "Failure mechanisms of high strength steels in bicarbonate solutions under anodic polarization." *Corros. Sci.*, 45, 2017–2030.

PTI. (1998). *Acceptance standards for post-tensioning systems*, Post-Tensioning Institute, Phoenix.

Sanchez, J., Fullea, J., Andrade, C., and Alonso, C. (2007). "Stress corrosion cracking mechanism of prestressing steels in bicarbonate solutions." *Corros. Sci.*, 49, 4069–4080.

Schupack, M. (2004). "PT grout: Bleedwater voids." *Concr. Int.*, 26(8), 69–77.

Trejo, D., et al. (2009a). "Effects of voids in grouted, post-tensioned, concrete bridge construction." *Rep. No. 0-4588*, Texas Transportation Institute, Texas Dept. of Transportation, Austin, Tex.

Trejo, D., Pillai, R. G., Hueste, M. D., Reinschmidt, K., and Gardoni, P. (2009b). "Parameters influencing corrosion and tension capacity of post-tensioning strands." *ACI Mater. J.*, 106(2), 144–153.

Vu, N. A., Castel, A., and Francois, R. (2009). "Effect of stress corrosion cracking on stress-strain response of steel wires used in prestressed concrete beams." *Corros. Sci.*, 51, 1453–1459.

Woodward, R. J., Cullington, D. W., and Lane, J. S. (2001). "Strategies for the management of post-tensioned concrete bridges." *Current and future trends in bridge design, construction, and maintenance—2*, P. C. Das, D. M. Frangopol, and A. S. Nowak, eds., Thomas Telford, London, 23–32.